Ischemic brains regenerate vascular mural pericytes by recycling detached endothelial cells, depending on TGFβ signaling

Tingbo Li[1], Qingzhu Gao[2], Xuzhao Li[2], Zhu Zhu[2], Yuxiao Jin[2], Yiyi Zhang[2], Jiongfang Xie[3], Peiran Zhu[4], Bingrui, Zhao[2], Jie-Min Jia*[2, 5, 6, 7]

[1]College of Life Sciences, Zhejiang University, Hangzhou, Zhejiang, 310058, China.

[2]Laboratory of Neurovascular Biology, School of Life Sciences, Westlake University, Hangzhou, 310024, China.

[3]Key Laboratory of Structural Biology of Zhejiang Province, School of Life Sciences, Westlake University, Hangzhou, Zhejiang, 310024, China.

[4]School of Materials Science and Engineering, Zhejiang University, Hangzhou, China.

[5] Westlake Laboratory of Life Sciences and Biomedicine, Hangzhou, 310024, China

[6]Key Laboratory of Growth Regulation and Translational Research of Zhejiang Province, School of Life Sciences, Westlake University, Hangzhou, 310024, China.

[7]Institute of Basic Medical Sciences, Westlake Institute for Advanced Study, Hangzhou, 310024, China.

*Correspondence: jiajiemin@westlake.edu.cn

Cerebral endothelial cells (ECs) fate and cellular sources for pericyte regeneration after stroke are unclear. by genetic tracing, we identified ECs undergoing cell-fate changing, likely through TGFβ-mediated transdifferentiation, into pericytes. Some of the migrating pericytes induced by stroke are derived from detached ECs. The EC-transformed pericytes can integrate into vasculature again, suggesting ischemic brains can recycle ECs from unfunctional vessels to replenish lost pericytes as an innate self-maintenance program sustaining repair phenomena.

Stroke kills millions each year and no effective treatment is available so far[1]. Brains possess an intrinsic, limited self-repair capacity[2, 3], e.g. spontaneous angiogenesis after stroke. However, understanding the definitive spontaneous repairing processes is largely incomplete. ECs form vascular tubes, while pericytes encircle the endothelial tube. The observation that more pericytes die faster than ECs may explain neurodegeneration exacerbation and brain self-recovery hindering after stroke because pericytes are a type of mural cells known to be critical for the blood-brain barrier and cerebral blood flow[4-6]. However, little is known about cellular sources for pericyte regeneration in the adult ischemic brain while it has been well documented that the cephalic neural crest gives rise to pericytes in all blood vessels of the face and forebrain during embryonic development[7, 8]. Many capillaries collapse after stroke, however, the fate of endothelial cells from these unfunctional vessels to be recycled or to die is unclear. Recently, Yu et al. have demonstrated that pericytes can be differentiated locally from a subgroup of ECs in multiple tissues under homeostasis[9]. However, the case in brains with or without ischemia remains unknown. Identification of origin cells for regenerated pericytes and EC's fate in

42 the ischemic brain is of importance for enhancing endogenous capacity to repair a stroke-
43 damaged brain.

44 To test if cerebral ECs differentiate into pericytes during adult angiogenesis as do those
45 in the mammary gland, skin, and retina[9], we employed a cell fate tracing system by
46 crossing EC-specific DNA recombinase driver line *Cdh5-CreERT2*[10] with triple EGFP
47 reporter (Ai47)[11] or tdTomato reporter (Ai14) (The Jackson Laboratory) (Fig. 1a). ECs and
48 their potential progeny cells are permanently labeled by EGFP or tdTomato fluorescent
49 proteins once tamoxifen (TAM) is provided (Extended Data Fig.1a). Consistent with
50 previous reports[9, 10, 12], these fluorescent proteins were restricted in ECs but not in any
51 other types of brain cells short-term after TAM exposure (4 - 7 days, Extended Data Fig.
52 1c-g). Upon long-term TAM exposure (Fig. 1b), although some of these $EGFP^+$ ECs in skin
53 tissue change their fates into $EGFP^+$ pericytes[9], brain $EGFP^+$ ECs, however, seemed never
54 (Fig. 1c-i). By using immunofluorescent staining of typical pericyte markers (CD13 and
55 PDGFRβ), we did not observe any $EGFP^+$ pericytes at various tracing periods, ranging
56 from 1.5 to 17.6 months (Fig. 1c-d, i). Whereas, all $EGFP^+$ cells remained expressing
57 multiple classical endothelial markers, such as CD31, VE-cadherin, ERG, and GluT1,
58 despite up to a two-year tracing (Fig.1e-i). Together, these results demonstrated unlike in
59 the peripheral system and retina, cerebral ECs are not the cellular source for pericytes in
60 adult brains under homeostasis.

61 Ischemic stroke, modeled by middle cerebral artery occlusion (MCAO, Extended Data
62 Fig. 2), induced cerebral ECs detaching from vessels, gradually losing EC markers, basal
63 membrane protein, and undergoing drastic morphological changes such as losing hollow

structure and growing multiple processes from cell soma (Fig. 1j-k and Extended Data Fig. 3a). This finding suggested that ECs might undergo cell fate changing in response to ischemia attack. Thus, we referred to this subgroup of EGFP$^+$ cells as 'EGFP$^+$ non-EC cells'. TAM was delivered to 1.5-month-old mice and then at least two weeks later we performed MCAO surgery (Fig. 1b), aiming to ensure no extra residual TAM. After 2-hour MCAO, sutures were withdrawn, permitting various periods of reperfusion, ranging from 8 all the way through 514 days (RP2D to RP514D) (Fig. 1b). These EGFP$^+$ non-EC cells can be found anywhere possible in the ischemic region, showing no regional specificity (Extended Data Fig. 3b). According to whether having secondary processes, we classified EGFP$^+$ non-EC cells into two types: type I, short, and fewer primary processes, no secondary processes (Fig. 1j, l, Extended Data Fig. 3c-e); type II, longer and more primary branches with secondary ones (Fig. 1k, l, Extended Data Fig. 3c-e), while their cell bodies were comparable in shape and size (Extended Data Fig. 3e). We found that the prevalence of these two types of cells switched when reperfusion period prolonged. (Fig. 1l). This morphological switching suggests type I becoming type II gradually. The prevalence of EGPF$^+$ non-EC cells started to rise at RP8D, peaked by RP52D, and finally declined back to a low level (Fig. 1m). This curve suggested that these transformed avascular EGFP$^+$ non-EC cells may die or be recruited back to vessels, becoming vascular cells again. We termed this possibility a recycling process. Furthermore, FACS analysis performed on the peak day (RP52D) revealed an EGFP$^+$ butCD31 negative population (EGFP$^+$ non-EC cells, Fig. 1l). These EGFP$^+$ transformed cells accounted for ~0.4% of total EGFP$^+$ cells which included ECs and non-EC cells (Fig. 1m). *Cdh5-CreERT2* may label a small portion of

86 neutrophils and monocytes in the bone marrow and circulation[12] (Extended Data Fig. 4
87 a-b), which are known to enter brain parenchyma shortly after stroke onset but dies out[13].
88 To discriminate whether parenchyma EGFP$^+$ non-EC cells are derived from EGFP$^+$ bone
89 marrow cells in *Cdh5CreERT2;Ai47* mice, we introduced a viral expression system
90 restricted to ECs preventing EGFP expression in hematopoietic cells (Extended Data Fig.
91 4c-e). Specifically, we injected cranially the Cre-dependent *AAV-DIO-EGFP* virus to
92 *Cdh5-CreERT2* single-positive mice that do not carry *Ai47* or *Ai14* reporter (Extended
93 Data Fig. 4c), resulting in high labeling specificity to ECs (Extended Data Fig. 4f-g). Once
94 again, we found EGFP$^+$ ECs transforming into non-EC cells after stroke (Extended Data
95 Fig. 4h). Notably, some of these cells extended their long processes and enwrapped
96 capillaries, reminiscent of pericyte characteristics (Extended Data Fig. 4h). Independent
97 radiation experiment was implemented to exclude the same possibility, we replaced
98 *Cdh5CreERT2;Ai47* mice's bone marrow with wild type ones (Extended Data Fig. 5a-b).
99 Despite the depletion of EGFP$^+$ bone marrow cells under this circumstance (Extended
100 Data Fig. 5a-b), we still found comparable EGFP$^+$ non-EC cells in ischemic regions
101 (Extended Data Fig. 5c-f), demonstrating that EGFP$^+$ immune cells were not the cell
102 source of EGFP$^+$ non-EC cells in parenchyma. These results together indicate that a
103 small proportion (0.4%) of ECs detached from vessels in the parenchyma, lost EC
104 features, and changed their cellular identity after subjecting them to ischemia insult.

105 To assess whether these EGFP$^+$ non-EC cells are derived from vascular stem
106 endothelial cells as reported previously[9] which involves cell proliferation, we traced cell
107 division events by injecting EdU for consecutive 34 days. No single EGFP$^+$ non-ECs were
108 found to be EdU positive after examining 15 brain slices from two mice (Fig. 2a-b).

109 similarly, neither Ki67 signals were found (Fig. 2c-d). Thus, we concluded these EGFP$^+$
110 non-EC cells may not be progenies of stem cells, suggesting that a transdifferentiation
111 process may be required.

112 By employing a list of cell type markers, we identified that 90% of EGPF$^+$ non-EC cells
113 were pericytes (namely, 'EGFP$^+$ pericytes') as they were positive for typical pericyte
114 markers of CD13, PDGFRβ, and NG2 (Fig. 3a-g), as well as that they were negative for all
115 of the markers of immature and mature neurons (doublecortin and NeuN), astrocytes
116 (GFAP), CNS macrophages (Iba1, CD68, and F4/80), myeloid cells (CD45), and smooth
117 muscle cells (α-SMA) (Extended Data Fig. 6a). The cell identity of the rest 10% of EGFP+
118 non-EC cells remained unknown (Fig. 3g) though as these cells were not labeled by any
119 cell markers that we used. Furthermore, more than a quarter of EGFP$^+$ pericytes were
120 recruited back to vessels (Fig. 3e-f and h, Movie1), suggesting ECs were fully recycled
121 not only by expressing pericyte markers but also by locating the right anatomical position.
122 A transformed tdTomato$^+$ non-ECs (here, Ai14 reporter was used instead of Ai47) that
123 were also tracked by *AAV-DIO-EGFP* virus exhibited one process attaching a capillary
124 while the other did not (Extended Data Fig. 6b), implying capturing a recruiting moment.
125 It has been repeatedly reported that pericytes detach from vessels after stroke[14]. We
126 found actually a third of these avascular, migrating pericytes were derived from ECs (Fig.
127 3i). Further analysis revealed that 23.3% of total vascular pericytes were EGFP$^+$ (Fig. 3h),
128 suggesting ECs are a fair contributor cell source for pericyte regeneration. The virus-
129 tracked ECs also can generate pericytes, coinciding with results from genetic tracing
130 (Extended Data Fig. 6c-d). These results together demonstrate that after ischemic stroke,

131 ECs transdifferentiated into pericytes, likely capable of integrating back into the cerebral
132 vasculature.

133 In addition, during EdU assay, we found that there were EdU positive pericytes that
134 were EGFP negative in both vascular and migrating pericytes (Fig. 3k), suggesting
135 alternate cell sources for pericyte regeneration except for EC transdifferentiation. Each
136 source contributed 20% of pericytes respectively (Fig. 3l). Therefore, we inferred that at
137 RP34D, 40% of total pericytes in ischemic regions were not pre-existing ones but
138 regenerated ones (Fig. 3l). Together, these findings indicated that ischemic brains have
139 more than one way to replenish pericytes when exerting self-repair after injury.

140 Next, we investigate the potential molecular signaling pathway that might mediate this
141 EC-to-pericyte transdifferentiation. Since TGFβ signaling is well documented for cell fate
142 changing including the endothelial mesenchymal transition (EndMT) process, a newly
143 recognized type of transdifferentiation[15, 16]. Therefore, we injected LY364947, a TGFβRI
144 inhibitor when MCAO was performed, followed by additional daily injections for
145 consecutive 34 days of reperfusion. We found significantly fewer $EGFP^+$ non-EC cells
146 appeared overall (Extended Data Fig. 6e-f). FACS analysis further confirmed this
147 conclusion quantitively (Fig. 3m-n). These results strongly suggested that TGFβ signaling
148 in ECs is centrally important. Together, under ischemic conditions, ECs exploited TGFβ
149 signaling to transform ECs into pericytes during reperfusion to replenish the shrunk
150 pericyte pool occurring in the acute ischemia period.

151 Overall, using mouse genetic tracing tools combined with virus infection and
152 pharmacology, we demonstrated adult ischemic brains spontaneously repair

153 microvasculatures by regenerating new pericytes that are transformed from ECs after
154 detaching from vessels. Distinct from the previous findings in peripheral organs in which
155 a small group of endothelial stem cells Procr+ ECs differentiate into pericytes during adult
156 angiogenesis under homeostasis[9], ECs do not become pericytes in normal brains but
157 transdifferentiate into pericytes without cell division. The death rate is dozens of times
158 higher in pericytes than in ECs within 24 hours after a transient focal ischemia[4],
159 suggesting abundant capillaries become damaged by being naked. What is the fate of
160 these naked capillaries made up by ECs? The present study suggests that these naked
161 vessels may release ECs, some of which may not die but rather be recycled and
162 repurposed by the ischemic brain. By observing type I simpler form switching to type II
163 more complex EGFP+ non-EC cells (Fig. 1l) and the medium stage of the transformed
164 EFGP+ pericyte (Extended Data Fig. 6b), we extrapolate them likely being recruited and
165 serve as building blocks to repair the existing damaged vasculatures. This could be an
166 efficient system to reuse brain cells that have lost their original functions. Further studies
167 are required to live imaging the whole dynamic process during reperfusion periods.

168 Identifying new cellular sources for pericyte replenishment is important not only for
169 stroke but also for many other either acute or chronic brain injuries. This study may
170 suggest a novel therapy for generating EC-derived pericyte without involving stemness
171 which has long been a concern for tumorigenesis.

172 **Methods**

173 **Experimental design**. Transgenic Cdh5CreERT2 transgenic mice[10] cross with reporter
174 mice *Ai47 (EGFP$^{f/f}$) reporter* or *Ai14 (tdTomato$^{f/f}$) reporter mice*. Thus, ECs are labeled in
175 green or red initially. TAM was delivered when mice were 1.5 months old (6 weeks), i. e.

genetic tracing started. After waiting for 2 weeks, MCAO was performed. After a 2-hour occlusion, reperfusion began. Contralateral sides of the ischemic brain were used as objects for homeostasis conditions, except for the time point of tracing 4 days. Thus, it was traced for 22 days in the PR8D mice (N = 3 mice), 1.6 months in RP34D (N = 27 mice), 2.8 months in RP71D (N = 3 mice), 14 months in RP408D (N = X mice), 8.2 months in RP232D (N = 3 mice), 14 months in RP408D (N = 2 mice),17.6 months in RP51D mice (N = 2 mice). The tracing time point of 1.6 months (RP34D) was the most frequently examined. FACS and immunohistochemistry were the major two techniques used for cell identity confirmation.

Animal care and tissue dissection.

All animal experiments were carried out in accordance with protocols approved by the Institutional Animal Care and Use Committee (IACUC) at the School of Life Sciences, Westlake University. Wild-type C57BL6/J mice were purchased from the Laboratory Animal Resources Center of Westlake University. Cdh5CreERT2 mice were a gift from Le-Ming Zheng (Peking University). Gt(ROSA)26Sor$^{tm47(CAG\text{-}EGFP^{*})Hze}$ (Ai47) was share by Zilong Qiu (ION). We crossed Cdh5Cre-ERT2 mice to Ai47 mice to generate Cdh5CreERT2:Ai47 mice. Standard chow and water were provided to mice *ad libitum*. Four mice were housed in each cage. All animals were housed in a standard animal room with a 12/12-hour light/dark cycle at 25 °C. Both male and female mice were used in this study. Mice were anaesthetized by intraperitoneal injection of 无巴比妥钠 (10 mg/kg?), and brain dissection was performed immediately for FACS experiments or cardiac PFA perfusion was performed for immunohistochemistry experiment. After fixation, brains

198 were dissected and kept in 4% PFA for additional 4 hours and then transferred to PBS
199 until further processing.

200 **MCAO**

201 Adult mice were anesthetized with pentobarbital sodium (100 mg/kg) and body
202 temperature was maintained during surgery with a heating pad. A midline neck incision
203 was made, the right common carotid artery was carefully separated from the vagus nerve,
204 and the artery was ligated using a 5.0-string. A second knot was made on the left external
205 carotid artery. The right internal carotid artery (ICA) was isolated, and a knot was left
206 loose with a 5.0-string. This knot was not tightened until the intraluminal insertion was
207 done. A small hole was cut on the common carotid artery before it was bifurcated to the
208 external carotid artery and ICA. A silicon-coated monofilament (tip diameter = 230 μm,
209 Doccol Corporation, 602256PK5Re) was gently advanced into the ICA until it stopped at
210 the origin of the MCA in the circle of Willis. The third knot on the ICA was closed to fix the
211 filament in position. During MCA occlusion (2 h), mice were kept in a warm cage in which
212 the temperature was maintained at 35 °C.

213 **Laser speckle contrast imaging (LSCI)**

214 LSCI provides a measure of blood flow velocity by quantifying the extent of blurring of
215 dynamic speckles caused by the motion of red blood cells through the vessels. Briefly,
216 mice were placed under an RFLSI III device (RWD Life Sciences) before and after the
217 suture was successfully inserted through CCA. The skull over both hemispheres was
218 exposed by making an incision along the midline of the scalp. When a 785 nm laser is
219 used to illuminate the brain, it produces a random interference effect that represented

220 blood flow in the form of a speckle pattern. Scattering light was detected by a charge-
221 coupled device (CCD) camera, and the images were acquired by custom software from
222 RWD Life Sciences Company. For each acquisition, a total of 160 images, each of which
223 measured 2048 ×2048 pixels, were collected at 16 Hz.

224 **Tamoxifen**

225 Tamoxifen, 10 mg/ml dissolved in 200 μl corn oil, was administrated intragastrically for 4
226 consecutive days. Prior to further experiments, fluorescent protein expressions in mouse
227 ear vasculatures were first examined. Tamoxifen was administrated at least 2 weeks
228 before MCAO surgery.

229 **Immunohistochemistry**

230 Cryosections of fixed mouse brains (50 μm) were handled free-floating and washed for
231 5 minutes in PBS prior to further procedures. Tissue sections were permeablized and
232 blocked in the PBS containing 0.5% Triton and 5% BSA at room temperature for 1 hour.
233 Then, brain sections were incubated with a different primary antibodies, including
234 CD31(1:400, BD, Cat# 557355), VE-Cadherin(1:200, BiCellScientific, Cat# 00105),
235 ERG(1:300, Sigma, Cat# ab110639), GLUT1 (1:300, Sigma, Cat# 07-1401), NeuN
236 (1:300, Merck, Cat# ABN90P), Doublefortin (1:300, Santa clus, Cat# sc-271390), Iba1
237 (1:300, HUABIO, Cat# ET1705-78), GFAP (1:300, Proteintech, Cat# CL488-60190),
238 PDGFRβ (1:300, ThermoFisher, Cat# 14-1402-82), NG2 (1:300, Merck, Cat# AB5320)
239 ,CD68 (1:300, BIO-RAD, Cat# MCA1957T), CD45-APC (1:200, Biogend, Cat# 103112),
240 Ki67 (1:300, thermoscientific, Cat# RM-9106-S0), F4/80 (1:300, Cell Signaling, Cat#
241 30325), CD13 (1:300, R&D system, Cat# AF2335), α-SMA-CY3 (1:300, Sigma, Cat#

242 C6198), which were all diluted in the blocking solution (1% percelin, 5% BSA, and 0.1%
243 Triton in PBS) at 4 °C overnight. After rinsing in PBS 3 times for 5 minutes each, brain
244 slices were incubated with secondary antibodies accordingly, including donkey anti-
245 mouse IgG (A21202, Thermo Fisher Scientific, 1:1,000) and donkey anti-rabbit IgG
246 (A10040, Thermo Fisher Scientific, 1:1,000). They were diluted in the blocking solution.
247 After a 2-hour incubation, brain slices were washed with PBS three times for 15 minutes
248 each. Finally, Hoechst counterstaining was performed for each specimen. After mounting
249 in an anti-fade mounting medium, images were acquired by using a Zeiss LSM800 laser-
250 scanning confocal microscope with a 20X or 63X objective, with or without Airyscan
251 mode.

252 **Flow cytometry**

253 Primary cell preparation was conducted as described below. Mouse brains were
254 dissected into cold HBSS with glucose and BSA ($HBSS^{++}$, Vendor info) were cut into small
255 pieces by sterile scissors, followed by a centrifuge at 1600 rpm/min for 5 mins to get rid
256 of supernatant. The minced tissues after the centrifuge were incubated with collagenase
257 IV (2.5 mg/ml, ROCHE, Cat# 11088858001) at 37 °C with gentle rotation for 30 min in
258 2 ml of $HBSS^{++}$. Next, samples were passed through a 70-μm filter and washed with
259 $HBSS^{++}$. To obtain higher cell yield, grind the tissue on the 70-μm filter using a syringe
260 piston and guarantee all tissue pass the filter. The following antibodies in 1:200 dilutions
261 were used: CD31-PE-594 (1:200, Biolegend, Cat# 102520), CD45-APC (1:200, Biogend,
262 Cat# 103112), Ly6C-APC (1:200, Biolegend, Cat# 128016), CD11b-PE (1:200,
263 Biolegend, Cat#101212), Viability dye (1:1000, ThermoFisher, Cat#65-0863-14).
264 Antibody incubation was performed on ice for 30min in HBSS with glucose and BSA. All

265 analyses were performed with CytoFLEX LX-5L1(Beckman). FlowJo x software was used
266 for data analyses.

267 **EdU injection**

268 EdU (200 mg/kg, Alfa Aesar Chemical) was injected intraperitoneally for consecutive 34
269 days since when MCAO was performed. EdU was initially dissolved in DMSO at the stock
270 concentration of XX mg/ml and was diluted with saline prior to injection.

271 **Virus injection**

272 The following adenovirus vector *AAV-CAG-DIO-EGFP* was purchased for ShuMi, Wuhan,
273 China (PT-0168). Half of the one-micron virus was delivered to postnatal day 2 mouse
274 pups by intracerebroventricular injection to both sides. After 1.5 months, tamoxifen was
275 administrated. One month later, these mice were subjected to MCAO to induce ischemic
276 stroke.

277 **Radiation and bone marrow transplantation**

278 At two weeks post tamoxifen injection, adult *Cdh5CreERT2:Ai47* mice received radiation
279 (total: 11Gy, 2 times, 5.5Gy per time, interval 2 hours) and bone marrow cell
280 transplantation from wild-type mice with the same genetic background. RBCs were
281 removed from the bone marrow cells by using ACK Lysis Buffer (4 Million cells/mouse).
282 These mice were subjected to MCAO 2 months after bone marrow reconstruction.

283 **Mouse cranial imaging by two-photon microscopy**

284 Adult mice were anesthetized with pentobarbital sodium, and analgesia was provided by
285 subcutaneous injection of 0.2% meloxicam. The scalp was removed, and the skull was

286 exposed and cleaned. A dental drill with a 0.6-mm-diameter bit was used to engrave and
287 thin the bone around the circular craniotomy area at a size of 3 mm. The piece of skull
288 was carefully peeled off with fine-pointed forceps, and a cranial window was generated.
289 A coverslip with a 3-mm diameter was placed on the cranial window, and its perimeter
290 was completely sealed with a 1% agarose gel. The metal headplate was glued onto skull
291 with dental acrylic, through which the mouse brain was fixed on a headplate holder. The
292 headplate holder together with the mouse was placed under a two-photon microscope
293 (FVMPE-RS, Olympus). The cerebral vasculature *Cdh5CreERT2:Ai47* mice was
294 visualized and imaged once a day before and after stroke. All surgeries were performed
295 with sterilized instruments and an environment.

296 **Statistics.**

297 The quantified data in all figures were analyzed with GraphPad Prism 7.0 (La Jolla, CA,
298 USA) and presented as the mean ± SEM with individual data points shown. Unpaired two-
299 tailed Student's t-test was used for assessing the statistical significance between two
300 groups. Statistical significance was determined by calculation of p-value (*$p < 0.05$, **$p <$
301 0.01, ***$p < 0.001$, and ****$p < 0.0001$, ns: not significant). The repetition of our data is
302 independent biological replicates and the number of replicates for each experiment is
303 noted in the corresponding figure legend.

304 **Data availability**

305 The source data underlying the graphs and charts shown in the figures and tables are
306 provided in Supplementary Data 1. All data generated or analyzed during this study are

307 included in this published article (and its supplementary information file).

308 **Acknowlegements**

309 We thank Xuzhao Li, Zhu Zhu, Dongdong Zhang, Jinze Li, Jiayu Ruan, Lili Zhou for their
310 constructive discussions. We thank Danping Lu for her responsive and timely purchasing
311 support, Jiongfang Xie for sharing AAV virus. We thank the animal facility for its technical
312 assistance with rodent housing, Biomedical Research center platform for technique
313 support. This work is supported by the National Natural Science Foundation of China
314 (31800864 and 31970969 to J.-M.J, 82101475 to Z.Z.), Westlake startup funds, Westlake
315 Education Foundation and MRIC funds (103536022011) to J.-M.J.; Westlake Education
316 Foundation to B.D.

317 **Author contributions**

318 J.-M.J. conceived the research. T.L. and J.-M.J. designed experiments. T.L. performed
319 all the experiments and data quantification, except for the virus cranial injection. Y.W.
320 performed FACS together with T.L.. Z.Z. conducted some stroke models. Q.G. and B.Z.
321 conducted mouse genotyping.

322 **Competing interests**

323 All authors declare no competing interests.

324

Fig. 1

Li et al.

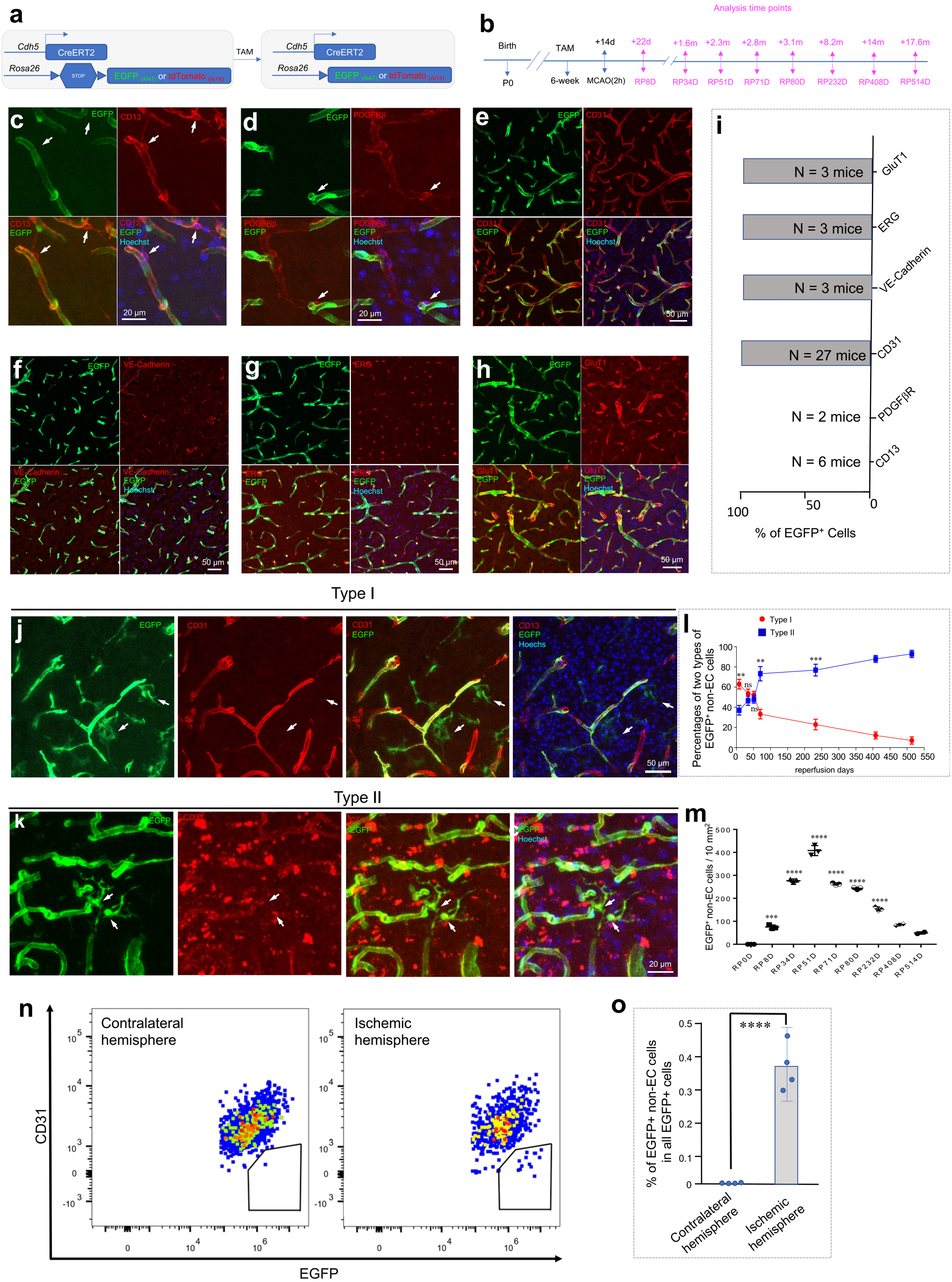
a
Cdh5
CreERT2
Rosa26
STOP
EGFP (Ai47) or tdTomato (Ai14)
TAM
b
Analysis time points
Birth
P0
TAM
6-week
+14d
MCAO(2h)
+22d
RP8D
+1.6m
RP34D
+2.3m
RP51D
+2.8m
RP71D
+3.1m
RP80D
+8.2m
RP232D
+14m
RP408D
+17.6m
RP514D
c
EGFP
CD13
d
PDGFRβ
e
CD31
f
VE-Cadherin
g
ERG
h
GluT1
Hoechst
20 μm
50 μm
i
N = 3 mice
GluT1
N = 3 mice
ERG
N = 3 mice
VE-Cadherin
N = 27 mice
CD31
N = 2 mice
PDGFβR
N = 6 mice
CD13
100
50
0
% of EGFP+ Cells
Type I
j
k
Type II
l
Type I
Type II
Percentages of two types of EGFP+ non-EC cells
reperfusion days
m
EGFP+ non-EC cells / 10 mm2
RP0D
RP8D
RP34D
RP51D
RP71D
RP80D
RP232D
RP408D
RP514D
n
Contralateral hemisphere
Ischemic hemisphere
CD31
EGFP
o
% of EGFP+ non-EC cells in all EGFP+ cells
Contralateral hemisphere
Ischemic hemisphere

Figure legends

Fig. 1 Genetic tracing of cerebral Cdh5$^+$ ECs demonstrates that they do not contribute to pericyte generation during adult angiogenesis but change cell fate to non-EC identity after ischemic stroke. a, Illustration of genetic tracing strategy using *Cdh5CreERT2;Ai47* or *Ai14* line. **b**, Experimental design for tracing periods and reperfusion periods following 2-hour ischemia. **c**-**h**, Confocal images of brain slice vasculatures traced for 1.6 months, stained with pericyte markers (CD13 and PDGFβR) and EC markers (CD31, VE-Cadherin, ERG, and GluT1). **i**, Summary of EGFP$^+$ cell's identity confirmation. CD13 antibody staining used brain slices from 6 mice, two mice for each time point of 1.6 months, 8.2 months, and 14 months; PDGFβR staining used two mouse brains traced for 1.6 months; Mice used for CD31 antibody staining was summarized after examining 27 mice that included all the time points shown in **b**; for VE-Cadherin, ERG, and GluT1 antibody staining, each of them used 3 mice that were traced for 1.6 months. **j**-**m**, Confocal images of ischemic brain region from mice at RP34D (correspondingly, trace period 1.6 months), showing type I (**j**) and type II(**k**) EGFP$^+$CD31$^-$ cells (named as EGFP$^+$ non-EC cells). **l**, Quantification of percentages of each type of EGFP$^+$ non-EC cells over different reperfusion periods. N = 3 mice for each time point, excepting only 2 mice for RP408D and RP514D. **m**, The time course of EGFP$^+$ non-EC cell densities in the ischemic regions. N = 3 mice for each time point, excepting only 2 mice for RP408D and RP514D. **n**, FACS analysis of EGFP$^+$ non-EC cells from contralateral control hemisphere (left plot) and ischemic side (right plot) of the same mouse at RP34D. **p**, Quantification of EGFP$^+$ non-EC cells for **o**. N = 4 mice. Data presented as mean ± SEM, ** $P < 0.01$, *** $P < 0.001$, **** $P < 0.0001$

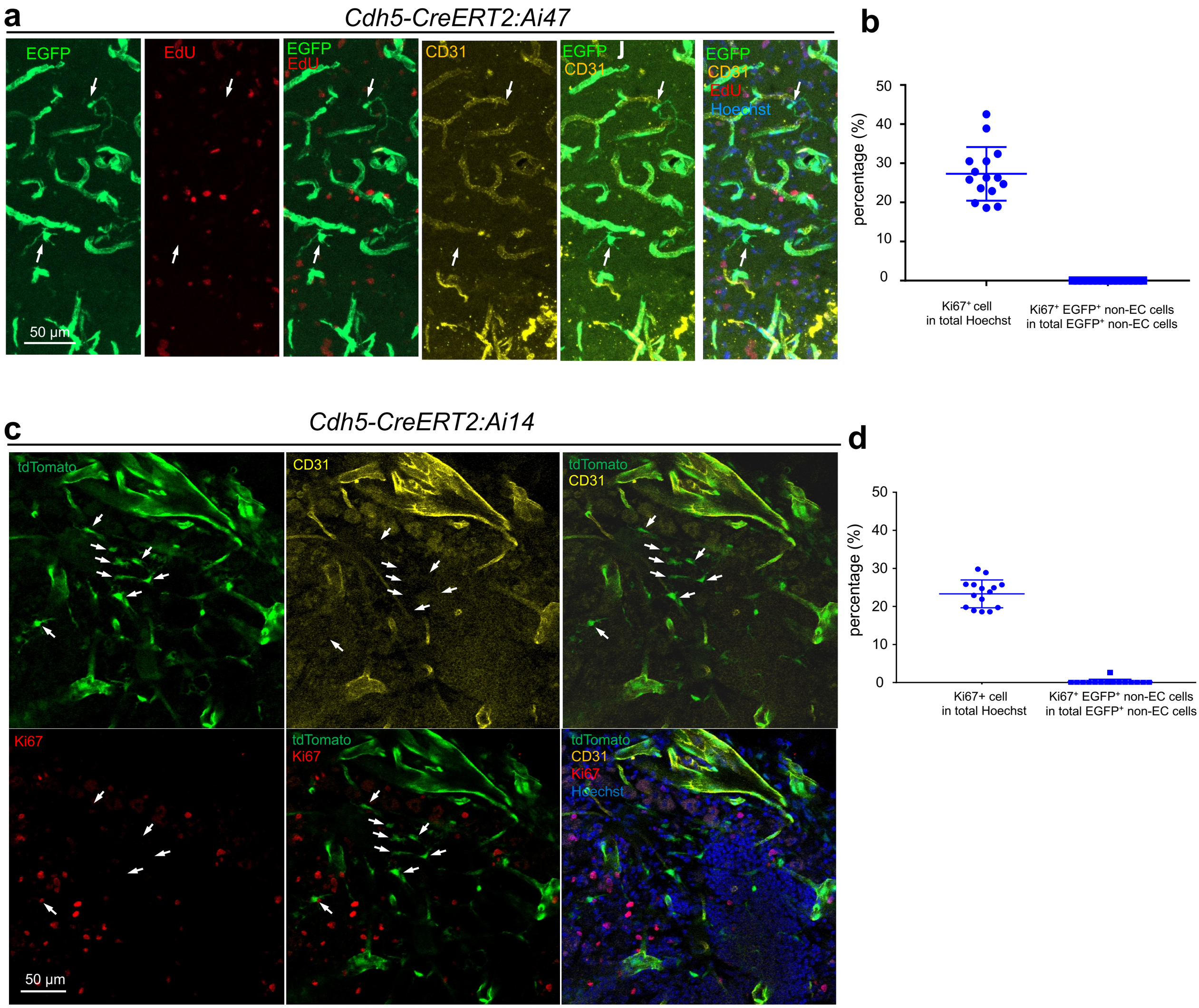
a
Cdh5-CreERT2:Ai47
EGFP
EdU
EGFP
EdU
CD31
EGFP
CD31
EGFP
CD31
EdU
Hoechst
50 μm
b
percentage (%)
50
40
30
20
10
0
Ki67+ cell
in total Hoechst
Ki67+ EGFP+ non-EC cells
in total EGFP+ non-EC cells
c
Cdh5-CreERT2:Ai14
tdTomato
CD31
tdTomato
CD31
Ki67
tdTomato
Ki67
tdTomato
CD31
Ki67
Hoechst
50 μm
d
percentage (%)
50
40
30
20
10
0
Ki67+ cell
in total Hoechst
Ki67+ EGFP+ non-EC cells
in total EGFP+ non-EC cells

348 **Fig. 2 EGFP$^+$ non-EC cell generation does not involve cell proliferation**. **a**,
349 Representative confocal images of a brain slice from the RP34D mouse that received
350 EdU daily injection for 34 days. **b**, Quantification of EdU$^+$ cells in total Hoechst$^+$ cell
351 population and EdU$^+$ EGFP$^+$ double positive and CD31$^-$ cells in the total EGFP$^+$ non-EC
352 cell population. n = 15 brain slices from two mice. **c**, Representative confocal images of
353 cell division marker Ki67 immunostaining from the RP34D mouse. **d**, Quantification of
354 Ki67$^+$ cells in total Hoechst$^+$ cell population and Ki67$^+$ EGFP$^+$ double positive and CD31$^-$
355 cells in the total EGFP$^+$ non-EC cell population. n = 15 brain slices from three mice.

356

Fig. 3

Li et al.

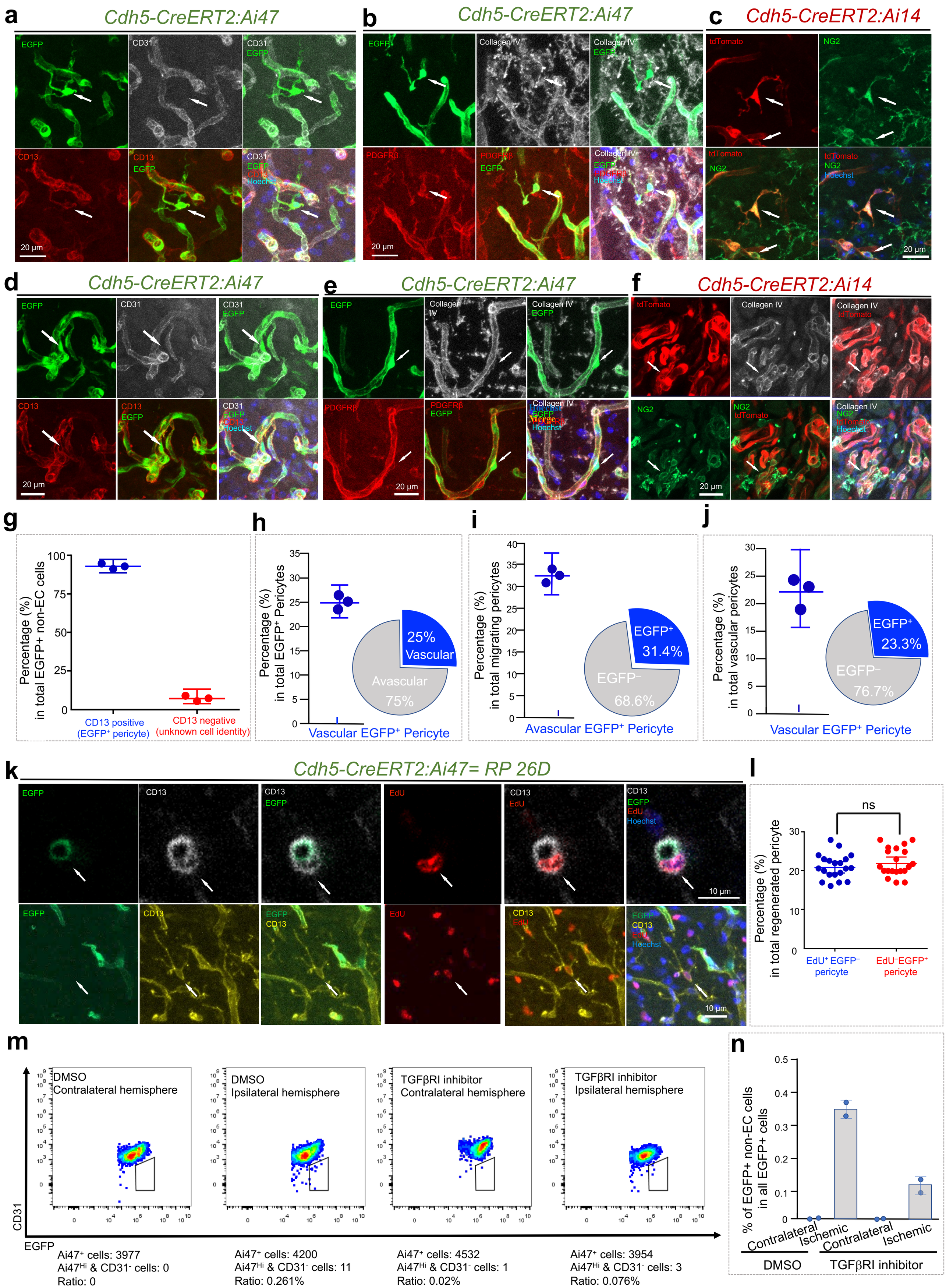
a
Cdh5-CreERT2:Ai47
EGFP
CD31
CD13
20 μm
b
Cdh5-CreERT2:Ai47
Collagen IV
PDGFRβ
c
Cdh5-CreERT2:Ai14
tdTomato
NG2
d
Cdh5-CreERT2:Ai47
e
Cdh5-CreERT2:Ai47
f
Cdh5-CreERT2:Ai14
g
Percentage (%) in total EGFP+ non-EC cells
CD13 positive (EGFP+ pericyte)
CD13 negative (unknown cell identity)
h
Percentage (%) in total EGFP+ Pericytes
25% Vascular
Avascular 75%
Vascular EGFP+ Pericyte
i
Percentage (%) in total migrating pericytes
EGFP+ 31.4%
EGFP− 68.6%
Avascular EGFP+ Pericyte
j
Percentage (%) in total vascular pericytes
EGFP+ 23.3%
EGFP− 76.7%
Vascular EGFP+ Pericyte
k
Cdh5-CreERT2:Ai47= RP 26D
EdU
10 μm
l
ns
Percentage (%) in total regenerated pericyte
EdU+ EGFP− pericyte
EdU−EGFP+ pericyte
m
DMSO Contralateral hemisphere
DMSO Ipsilateral hemisphere
TGFβRI inhibitor Contralateral hemisphere
TGFβRI inhibitor Ipsilateral hemisphere
CD31
EGFP
Ai47+ cells: 3977
Ai47Hi & CD31- cells: 0
Ratio: 0
Ai47+ cells: 4200
Ai47Hi & CD31- cells: 11
Ratio: 0.261%
Ai47+ cells: 4532
Ai47Hi & CD31- cells: 1
Ratio: 0.02%
Ai47+ cells: 3954
Ai47Hi & CD31- cells: 3
Ratio: 0.076%
n
% of EGFP+ non-EC cells in all EGFP+ cells
Contralateral
Ischemic
DMSO
TGFβRI inhibitor

357 **Fig. 3 Majority of EGFP$^+$ non-EC cells transdifferentiate into pericytes in the**
358 **ischemic brain, which was attenuated by TGFβRI inhibitor. a-f**, Representative
359 confocal images of avascular EGPF$^+$ pericytes (**a-c**) and vascular EGFP$^+$ pericytes (**d-f**).
360 **g**, The transforming efficiency of EGFP$^+$ non-EC cell to pericytes. **h**, Quantification of the
361 percentages of vascular and avascular EGFP$^+$ pericytes. N = 3 mice. **i**, The percentage
362 of avascular EGFP$^+$ pericytes in the total migrating pericyte population after stroke. **j**, The
363 contribution of vascular EGFP$^+$ pericytes to the total vascular pericyte population. **k**,
364 Confocal images of EGFP negative pericytes that were EdU positive after stroke. **l**, The
365 individual contributions of EGFP$^+$ & EdU$^-$ pericytes and EGFP$^-$ & EdU$^+$ pericytes to the
366 total pool of pericytes in ischemic regions. **m**, FACS plot comparison of EGFP$^+$ non-EC
367 cell number in mice that received daily injection DMSO or TGFβRI inhibitors for 34 days
368 since when MCAO was performed. **n**, Quantification for **m**. N = 2 mice. All the mice used
369 were at RP34D, correspondingly to the trace period of 1.6 months.

370

Extended Data Fig. 1

Li et al.

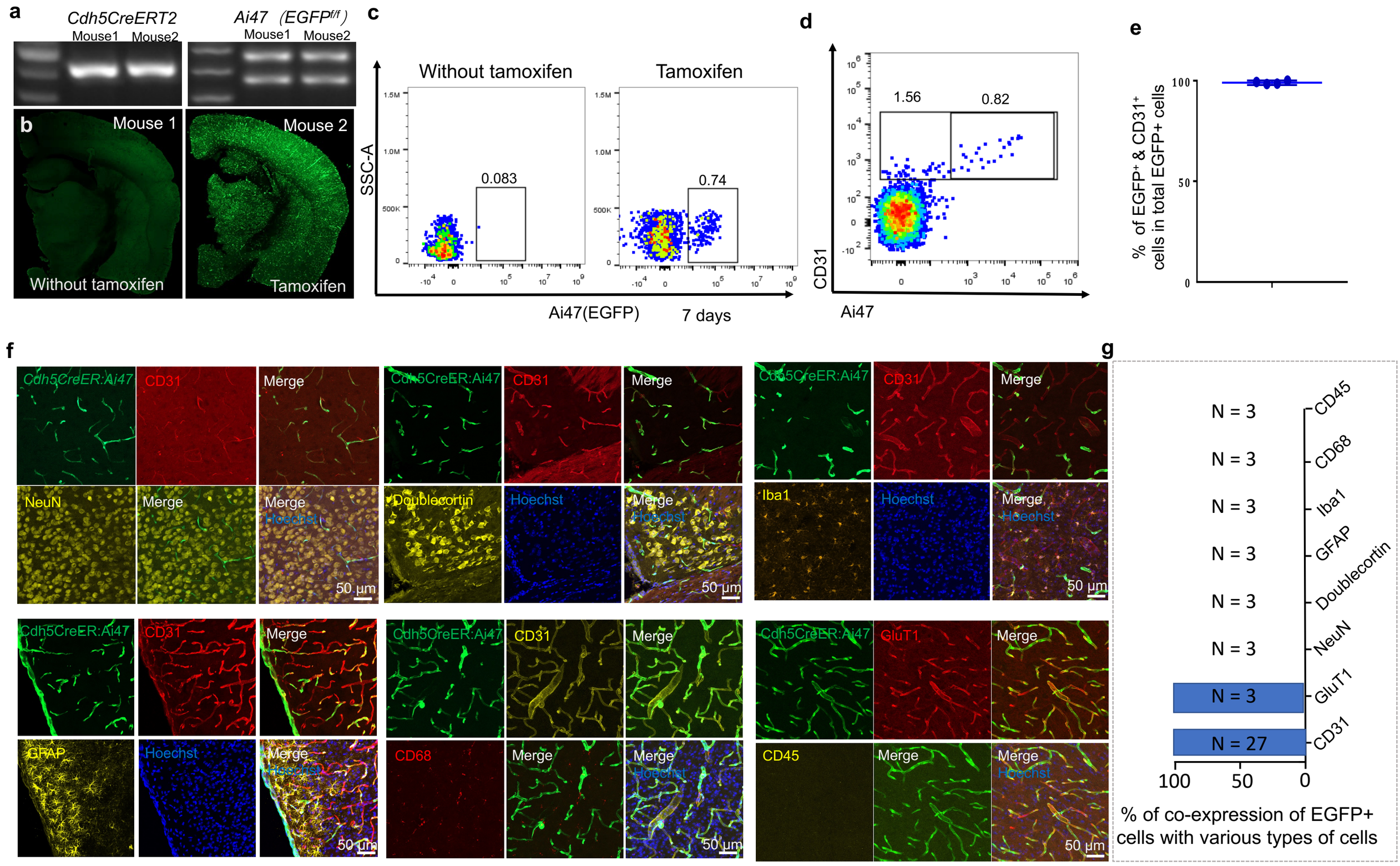

371 **Extended Data Fig. 1 The specificity of *Cdh5CreERT2* driver mouse line in ECs for**
372 **a 4-day tracing period. a-b**, Genotyping results of two *Cdh5CreER:Ai47* mice (**a**), one
373 with TAM injection (right in **b**) and the other with no TAM (left in **b**). c. FACS identification
374 of $EGFP^{-}$ and $EGFP^{+}$ cells population from individual two mice with TAM (right plot) or
375 without TAM injection (left plot). **d**, FACS analysis of EC labeling efficiency of TAX-
376 dependent EGFP expression. **e**. All $EGFP^{+}$ cells were $CD31^{+}$ at 1.6 months of the tracing
377 period. N = 4 mice. **f**. Confocal images of brain sections from *Cdh5CreER:Ai47* mouse
378 after staining with markers for a variety of cell types, NeuN for mature neurons,
379 doublecortin for immature neurons, Iba1 and CD68 for CNS macrophages, GFAP for
380 astrocytes, CD 45 for myeloid cells, and CD31 and GluT1 for ECs. **g**. Summary for **f**. N =
381 27 mice for CD31 and N = 3 mice for the rest of the markers.

382

Extended Data Fig. 2

Li et al.

a

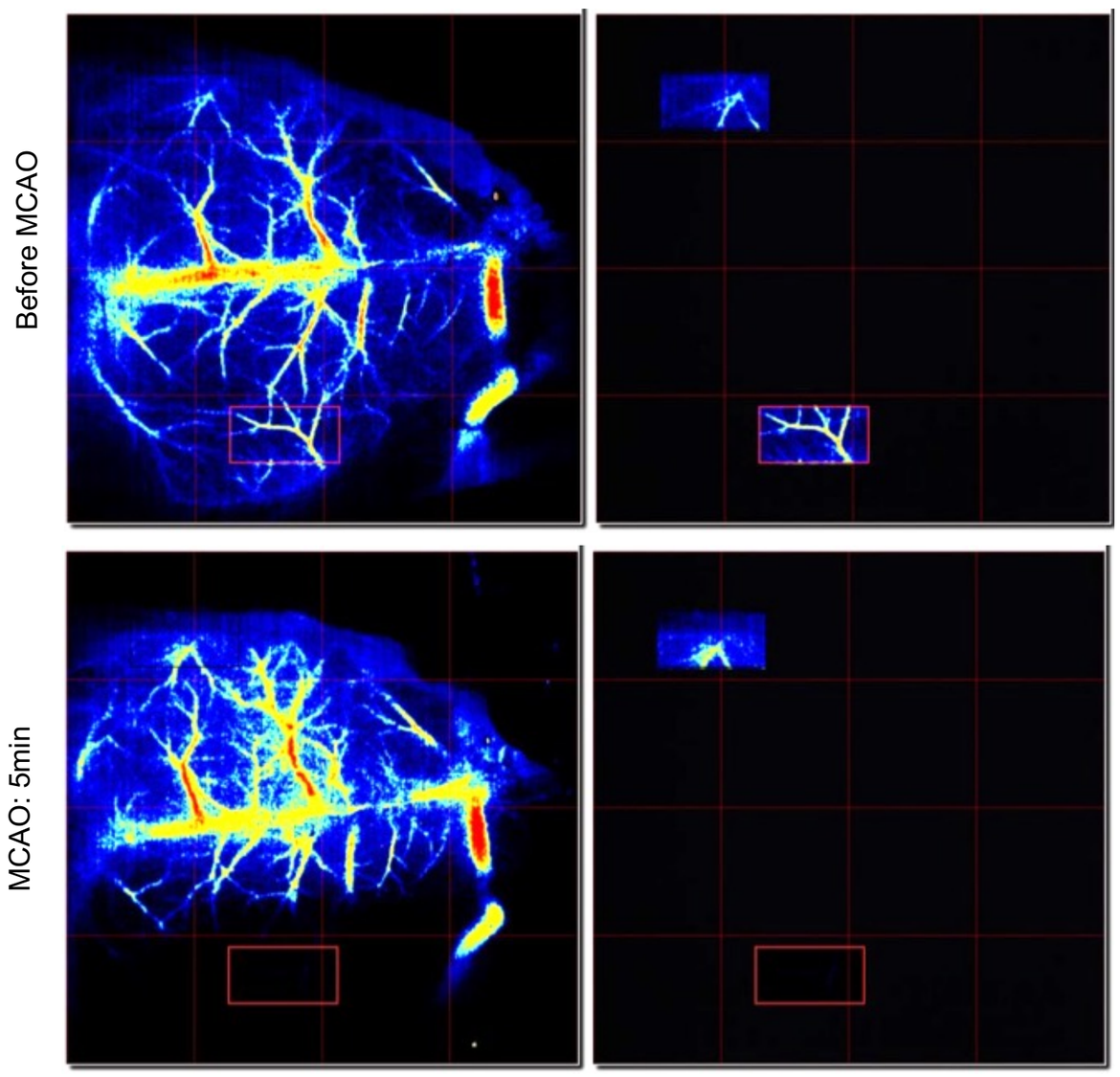

b

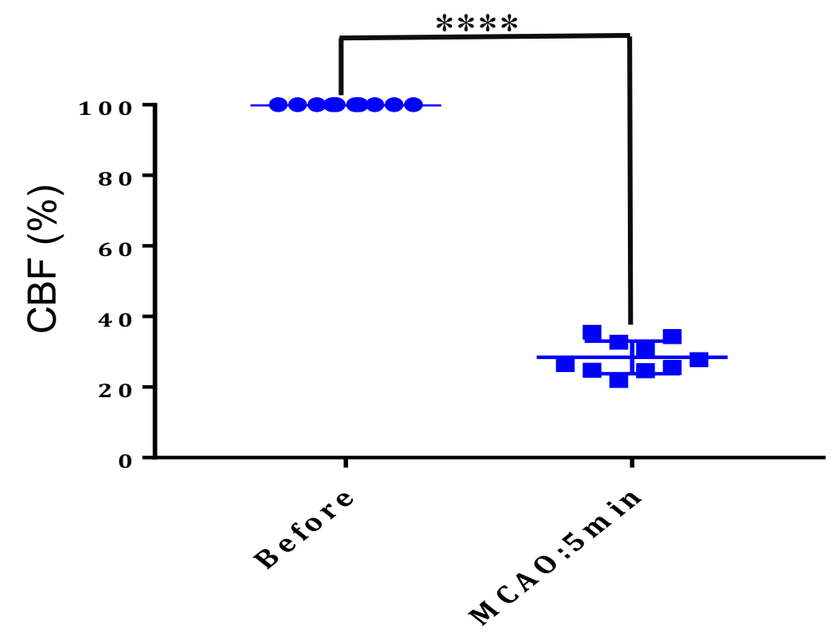

c

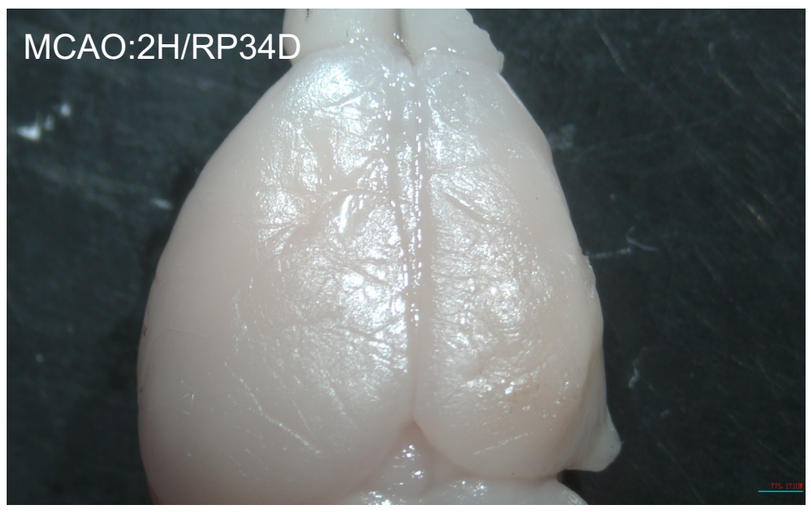

383 **Extended Data Fig. 2 Demonstration of successful MCAO for modeling stroke. a**,
384 Laser speckle contrast imaging of cerebral blood flow before and after MCAO. **b**,
385 Quantification of CBF reductions from 10 mice that were subjected to MCAO. **c**,
386 Representative bright field image of an atrophy mouse brain at RP34D. Data presented
387 as mean ± SEM, **** $P < 0.0001$

388

a

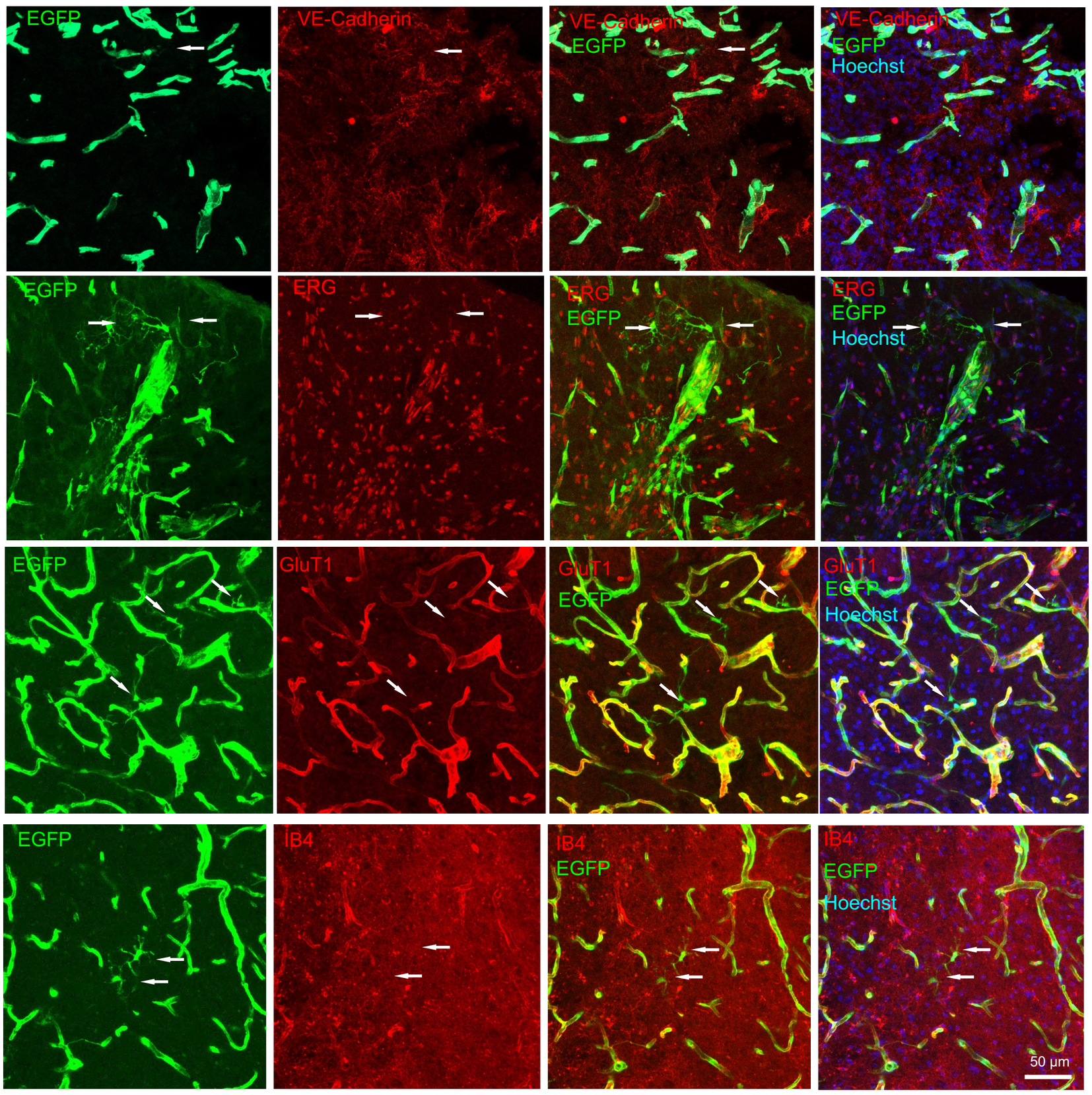
EGFP
VE-Cadherin
VE-Cadherin
EGFP
VE-Cadherin
EGFP
Hoechst
EGFP
ERG
ERG
EGFP
ERG
EGFP
Hoechst
EGFP
GluT1
GluT1
EGFP
GluT1
EGFP
Hoechst
EGFP
IB4
IB4
EGFP
IB4
EGFP
Hoechst
50 μm

b

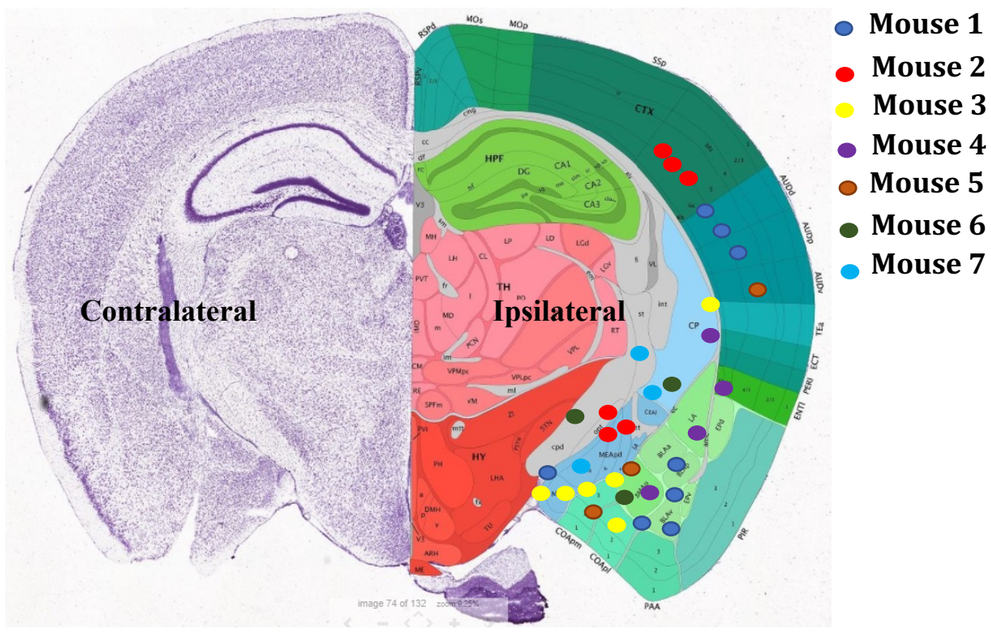
Contralateral
Ipsilateral
Mouse 1
Mouse 2
Mouse 3
Mouse 4
Mouse 5
Mouse 6
Mouse 7

c

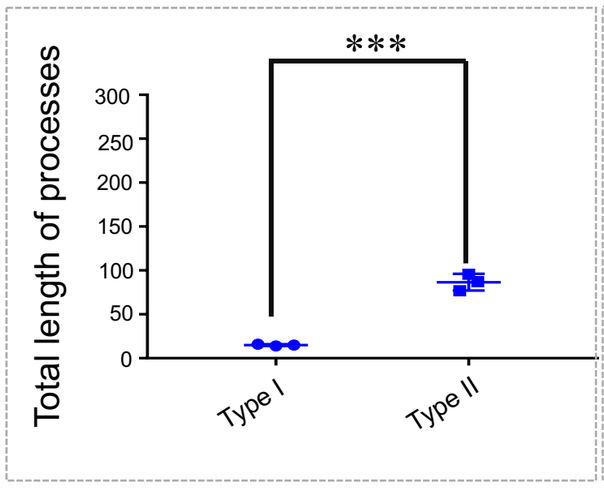
***
Total length of processes
300
250
200
150
100
50
0
Type I
Type II

d

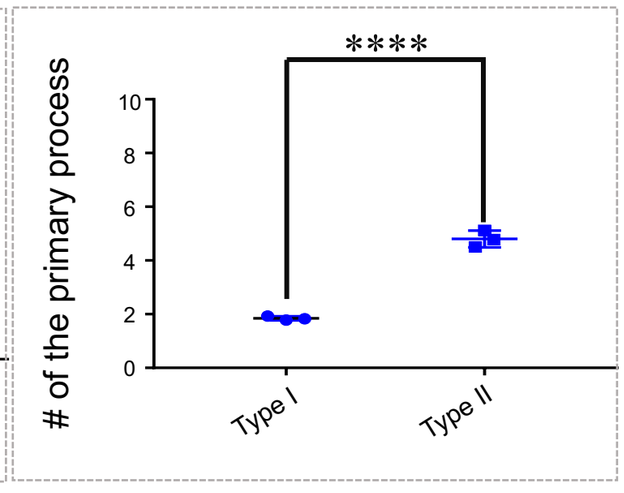
****
of the primary process
10
8
6
4
2
0
Type I
Type II

e

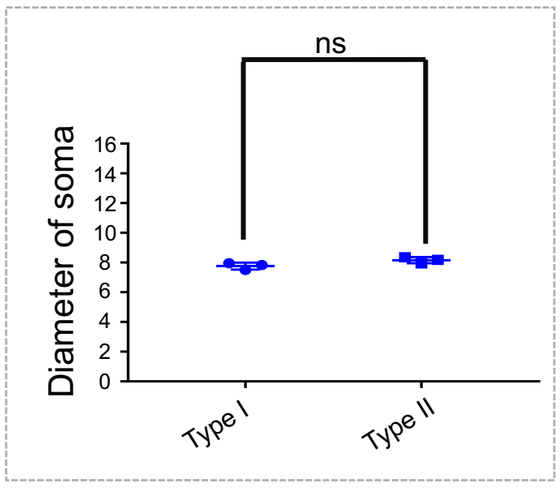
ns
Diameter of soma
16
14
12
10
8
6
4
2
0
Type I
Type II

389 **Extended Data Fig. 3 General characterizations of EGFP$^+$ non-EC cells. a**, Confocal
390 images of brain slices from mice at RP34D, stained by EC markers (GluT1, Ve-Cadherin,
391 and ERG), and basal membrane component IB4. White arrows indicate EGFP$^+$ non-EC
392 cells. **b**, An illustrative summary of anatomical locations of EGFP$^+$ non-EC cells after
393 examining 19 mice that included all the 8 time-points as shown Fig. 1**b**. **c**-**e**. Quantification
394 of the total process lengths (**c**), the number of primary processes (**d**), and the diameter
395 soma (**e**) for both type I and type II EGFP$^+$ non-EC cells. Data presented as mean ± SEM,
396 *** $P < 0.0001$, **** $P < 0.0001$

397

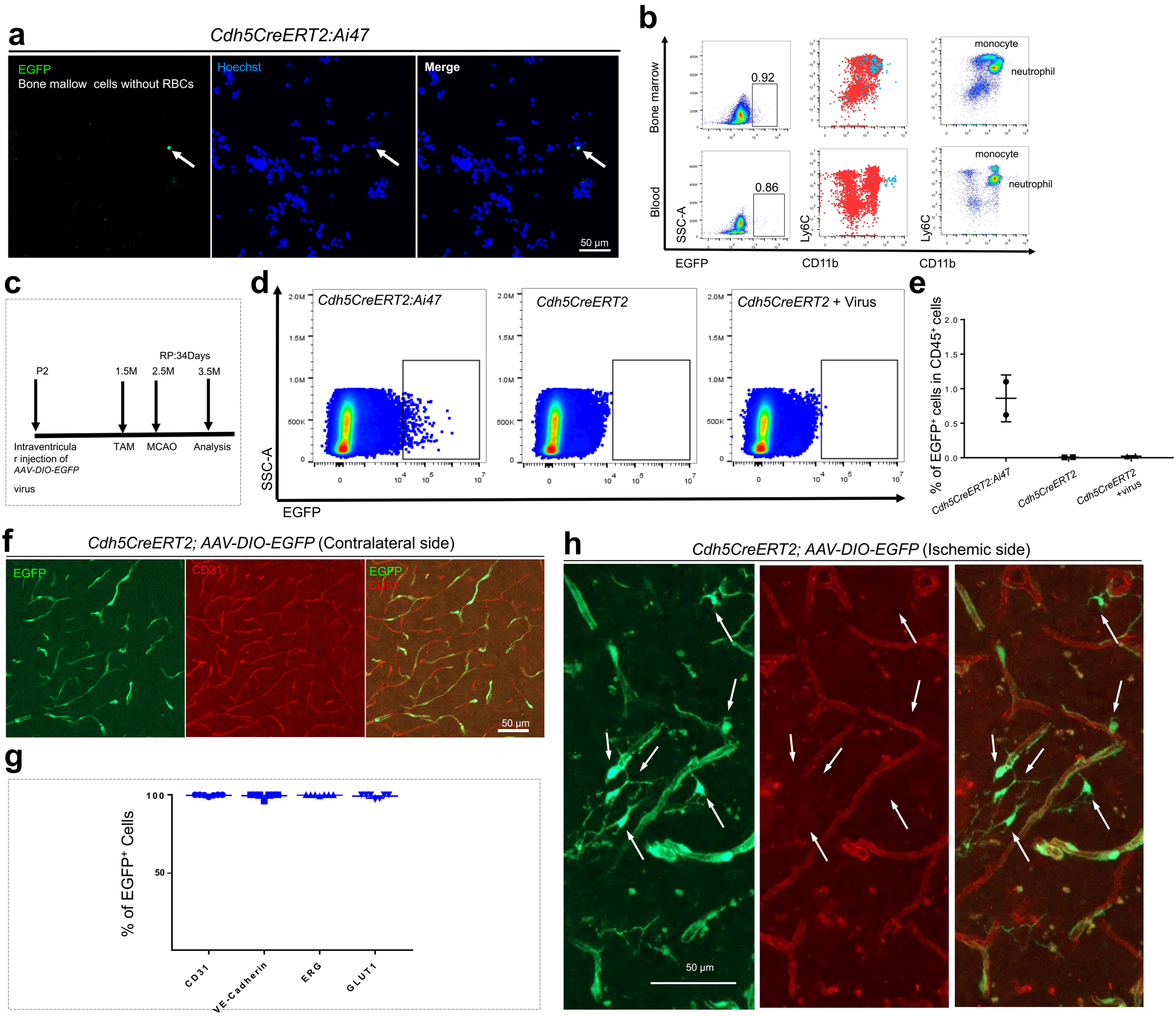
a
Cdh5CreERT2:Ai47
EGFP
Bone mallow cells without RBCs
Hoechst
Merge
50 μm
b
Bone marrow
Blood
0.92
0.86
monocyte
neutrophil
SSC-A
Ly6C
EGFP
CD11b
CD11b
c
RP:34Days
P2
1.5M
2.5M
3.5M
Intraventricular injection of AAV-DIO-EGFP virus
TAM
MCAO
Analysis
d
Cdh5CreERT2:Ai47
Cdh5CreERT2
Cdh5CreERT2 + Virus
SSC-A
EGFP
e
% of EGFP+ cells in CD45+ cells
Cdh5CreERT2:Ai47
Cdh5CreERT2
Cdh5CreERT2 +virus
f
Cdh5CreERT2; AAV-DIO-EGFP (Contralateral side)
EGFP
CD31
50 μm
g
% of EGFP+ Cells
CD31
VE-Cadherin
ERG
GLUT1
h
Cdh5CreERT2; AAV-DIO-EGFP (Ischemic side)
50 μm

398 **Extended Data Fig. 4 Exclusion of the possibility for Cdh5$^+$ peripheral circulating**
399 **cells to be the EGFP$^+$ non-EC cells found in parenchyma after stroke. a**, Wild-field
400 fluorescent images of white blood cells, stained with Hoechst, from *Cdh5CreERT2:Ai47*
401 mice. The white arrow indicates an EGFP$^+$ white blood cell. **b**, FACS analysis of the
402 EGFP$^+$ white blood cell identity in the bone marrow and circulating blood by using
403 neutrophil marker Ly6G and monocyte marker CD11b. Two independent experiments
404 were performed, resulting in the same conclusion. **c**, Illustration of *AAV-DIO-EGFP* virus
405 tracing strategy. **d**, FACS plots of EGFP+ cells in bone marrow cells from
406 *Cdh5CreERT2:Ai47*, *Cdh5CreERT2 alone, and Cdh5CreERT2* with virus injection. **e**,
407 Quantification of two independent experiments for **d**. **f**, EGFP expression in ECs after
408 virus infection in the contralateral side of *Cdh5CreERT2* mouse brain. **g**, Quantification
409 of EC markers in EGFP+ cells for f. **h**. EGFP$^+$ cells in the ischemic region of mice that
410 ECs were traced by virus labeling strategy. N = 7 brain slices from 1 mouse (trace period
411 1.6 months, RP34D) for **g**.

412

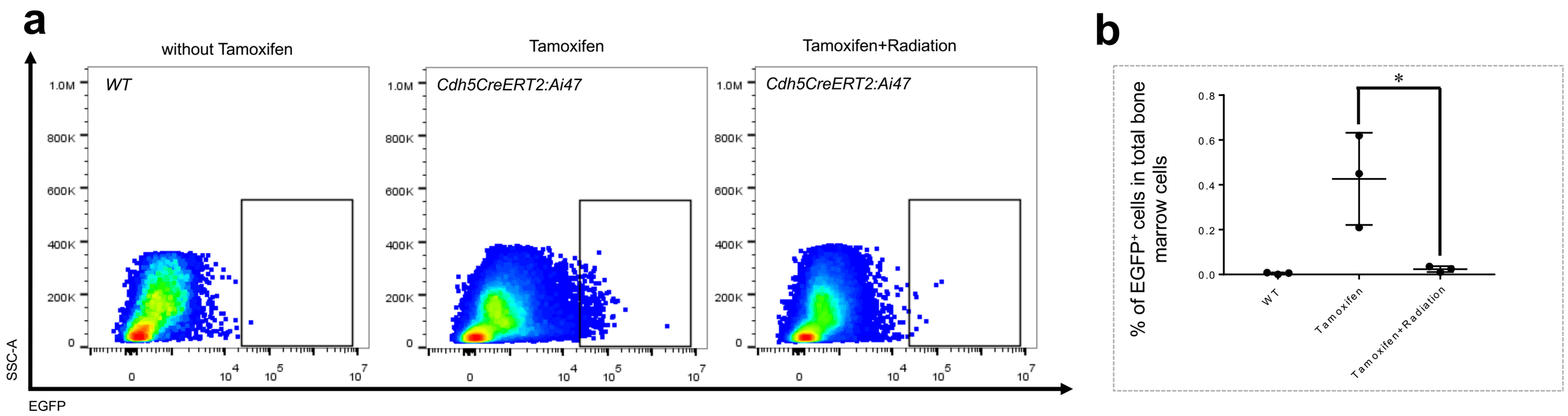
a
without Tamoxifen
Tamoxifen
Tamoxifen+Radiation
WT
Cdh5CreERT2:Ai47
Cdh5CreERT2:Ai47
SSC-A
EGFP
b
% of EGFP+ cells in total bone marrow cells
WT
Tamoxifen
Tamoxifen+Radiation
*

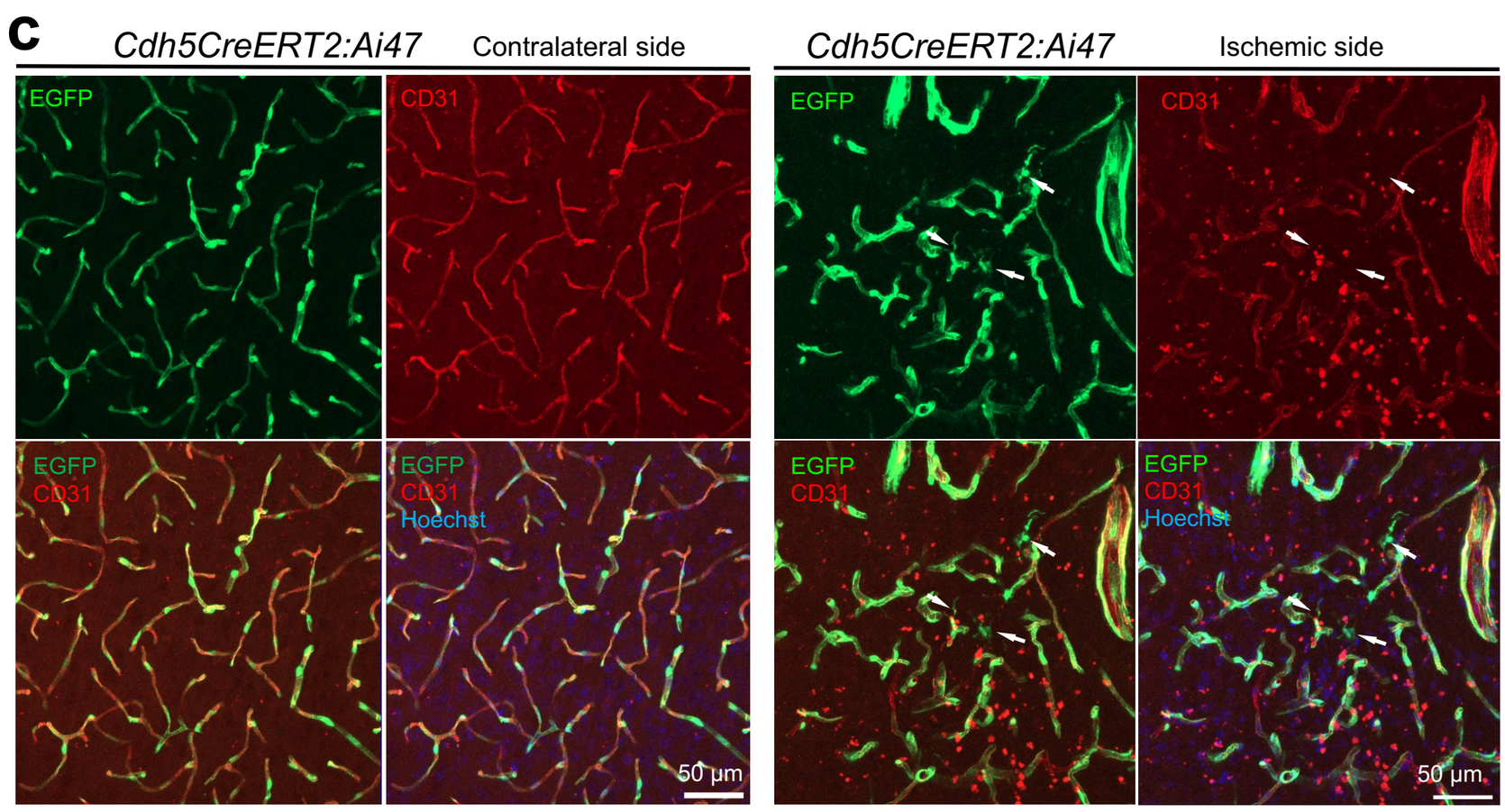
c
Cdh5CreERT2:Ai47
Contralateral side
Cdh5CreERT2:Ai47
Ischemic side
EGFP
CD31
Hoechst
50 μm

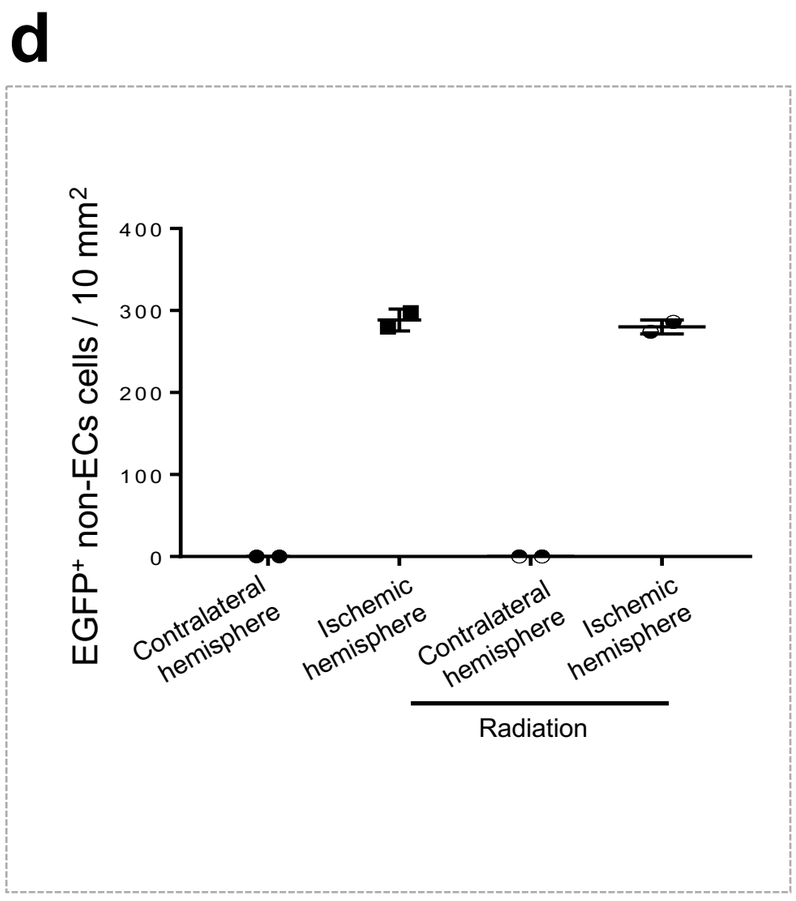
d
EGFP+ non-ECs cells / 10 mm2
Contralateral hemisphere
Ischemic hemisphere
Contralateral hemisphere
Ischemic hemisphere
Radiation

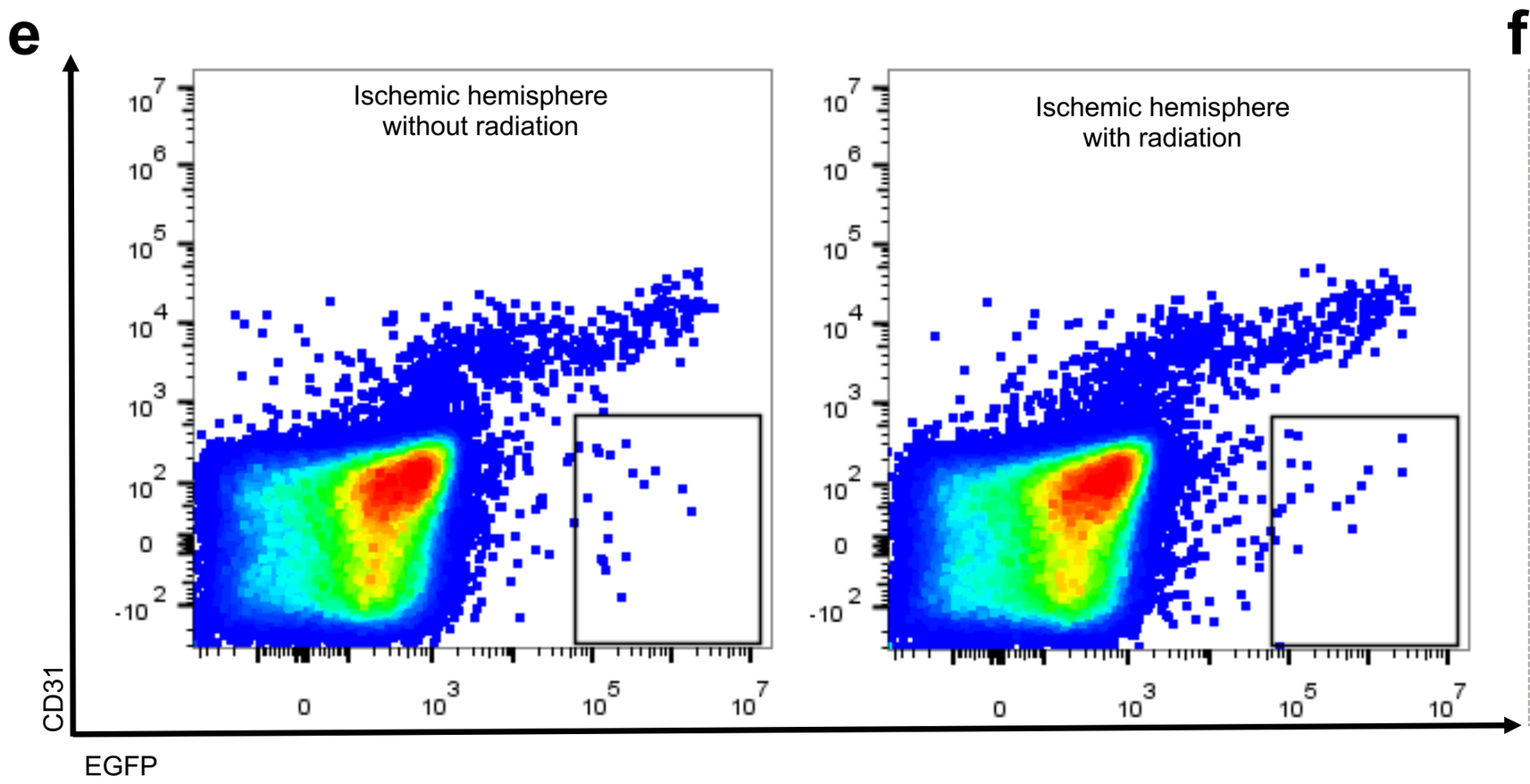
e
Ischemic hemisphere without radiation
Ischemic hemisphere with radiation
CD31
EGFP

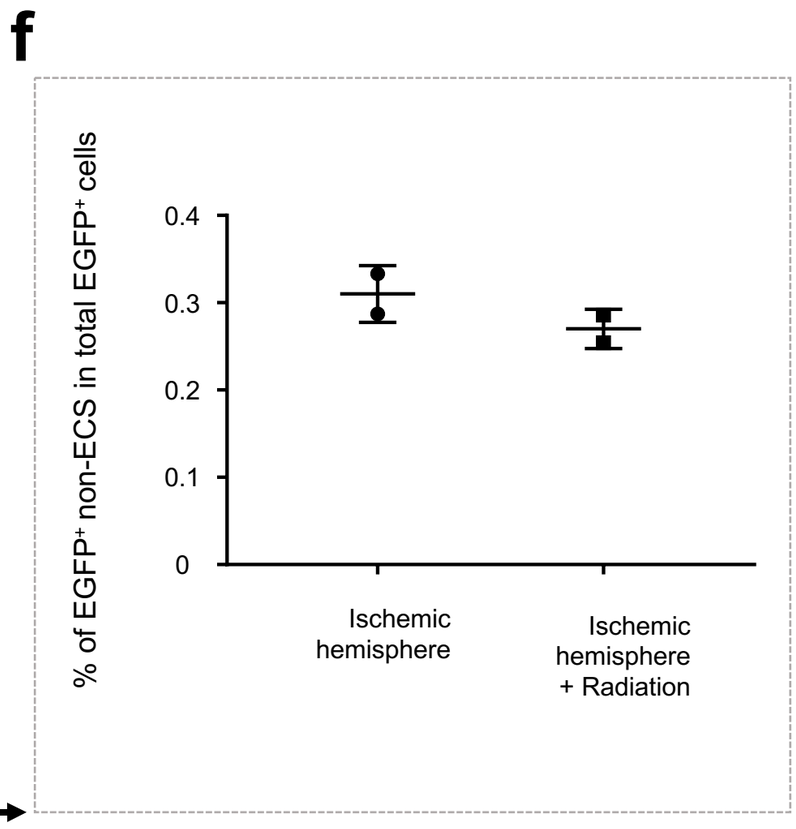
f
% of EGFP+ non-ECS in total EGFP+ cells
Ischemic hemisphere
Ischemic hemisphere + Radiation

413 **Extended Data Fig. 5 Radiation-depleted *Cdh5CreERT2;Ai47* mice exhibit EC cell**
414 **fate change.** **a**, FACS analysis of EGFP+ cells in three groups of *Cdh5CreERT2;Ai47*
415 mice that receive corn oil, TAM, or TAM together with radiation. **b**, Quantification for **a**, N
416 = 3 mice. **c**, Confocal images of vasculatures of the contralateral and ischemic side of the
417 brain from *Cdh5CreERT2;Ai47* mouse that received radiation. **d**, Quantification for **c**. N
418 = 2 mice. e-f, FACS analysis and quantification of EGFP+ non-EC cells in brains of mice
419 that received the same treatment as **c**. N =. 2 mice (trace period 1.6 months,
420 correspondingly RP34D). Data presented as mean ± SEM, * P < 0.05

421

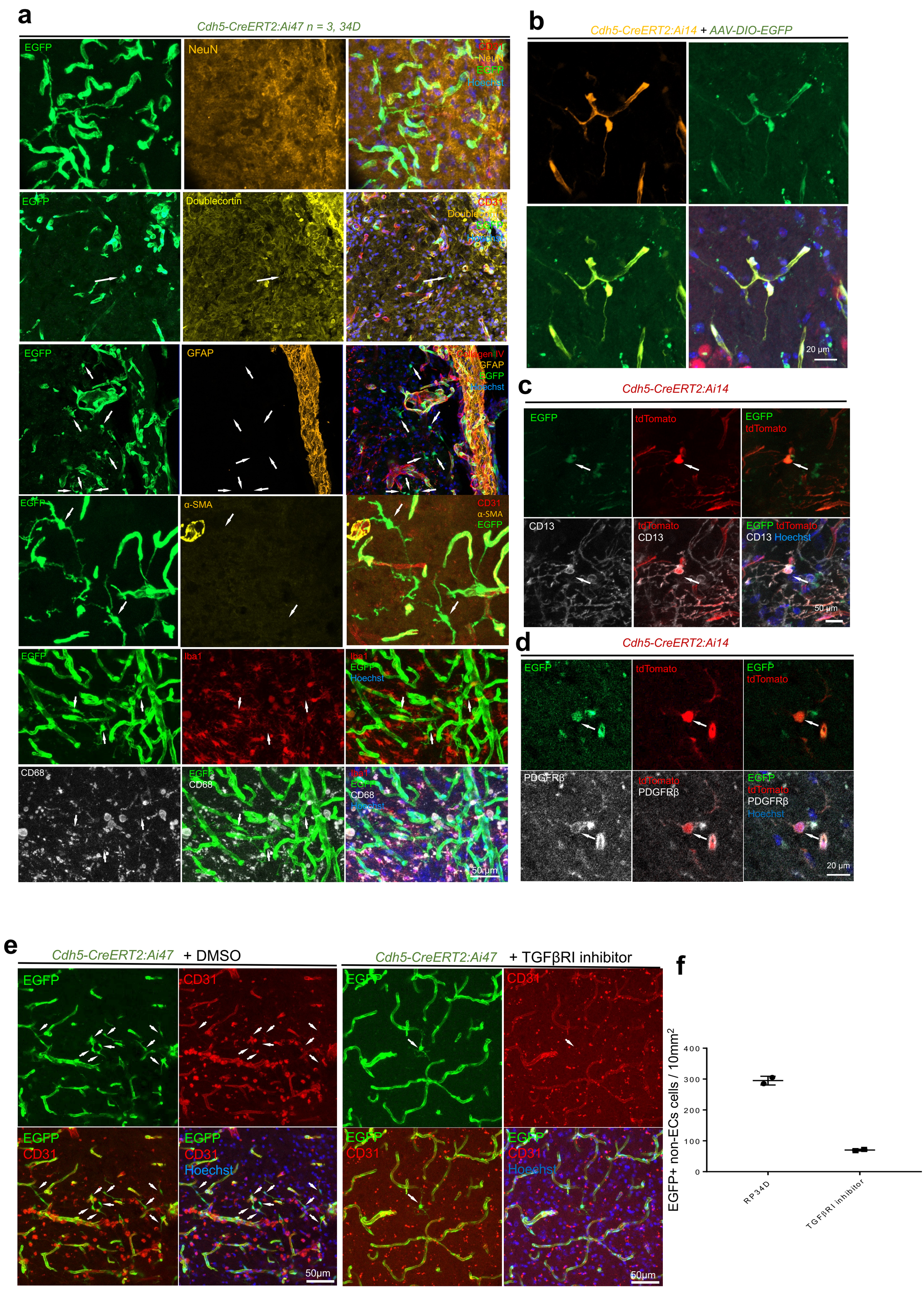
a
Cdh5-CreERT2:Ai47 n = 3, 34D
EGFP
NeuN
CD31
NeuN
EGFP
Hoechst
EGFP
Doublecortin
CD31
Doublecortin
EGFP
Hoechst
EGFP
GFAP
Collagen IV
GFAP
EGFP
Hoechst
EGFP
α-SMA
CD31
α-SMA
EGFP
EGFP
Iba1
Iba1
EGFP
Hoechst
CD68
EGFP
CD68
Iba1
EGFP
CD68
Hoechst
50 μm
b
Cdh5-CreERT2:Ai14 + AAV-DIO-EGFP
20 μm
c
Cdh5-CreERT2:Ai14
EGFP
tdTomato
EGFP
tdTomato
CD13
tdTomato
CD13
EGFP tdTomato
CD13 Hoechst
50 μm
d
Cdh5-CreERT2:Ai14
EGFP
tdTomato
EGFP
tdTomato
PDGFRβ
tdTomato
PDGFRβ
EGFP
tdTomato
PDGFRβ
Hoechst
20 μm
e
Cdh5-CreERT2:Ai47 + DMSO
Cdh5-CreERT2:Ai47 + TGFβRI inhibitor
EGFP
CD31
EGFP
CD31
EGFP
CD31
EGFP
CD31
Hoechst
50μm
EGFP
CD31
EGFP
CD31
Hoechst
50μm
f
EGFP+ non-ECs cells / 10mm2
400
300
200
100
0
RP34D
TGFβRI inhibitor

422 **Extended Data Fig. 6 EGFP$^+$ non-EC cells transformed into pericytes, depending**
423 **on TGFβ signaling cascade. a**, EGFP$^+$ non-EC cells were negative for a variety of cell
424 markers such as neurons (NeuN and doublecortin), astrocytes (GFAP), CNS macrophage
425 (Iba1), and SMC (α-SMA). **b**, A bipolar-shape EGFP$^+$ non-EC cell traced by the virus in
426 *Cdh5CreERT2:Ai14* mouse. **c**-**d**, EGFP$^+$ non-EC cells traced by the virus were positive
427 for pericyte markers (CD13 and PDGFβR). **e**. Brain sections from mice that were traced
428 for 1.6 months meanwhile received a daily injection of vehicle DMSO or TGFβRI inhibitors
429 since the day when MCAO was performed. **f**. Quantification of EGFP$^+$ non-EC cell
430 densities for **e**. N = 2 mice.

431 1. Kuriakose, D. & Xiao, Z. Pathophysiology and Treatment of Stroke: Present Status
432 and Future Perspectives. *Int J Mol Sci* **21** (2020).
433 2. Martino, G. How the brain repairs itself: new therapeutic strategies in inflammatory
434 and degenerative CNS disorders. *Lancet Neurol* **3**, 372-378 (2004).
435 3. Zhao, L.R. & Willing, A. Enhancing endogenous capacity to repair a stroke-
436 damaged brain: An evolving field for stroke research. *Prog Neurobiol* **163-164**, 5-
437 26 (2018).
438 4. Hall, C.N. *et al.* Capillary pericytes regulate cerebral blood flow in health and
439 disease. *Nature* **508**, 55-60 (2014).
440 5. Díaz-Flores, L., Gutiérrez, R., Varela, H., Rancel, N. & Valladares, F.
441 Microvascular pericytes: a review of their morphological and functional
442 characteristics. *Histol Histopathol* **6**, 269-286 (1991).
443 6. Pallone, T.L. & Silldorff, E.P. Pericyte regulation of renal medullary blood flow. *Exp*
444 *Nephrol* **9**, 165-170 (2001).

445 7. Simon, C., Lickert, H., Götz, M. & Dimou, L. Sox10-iCreERT2 : a mouse line to
446 inducibly trace the neural crest and oligodendrocyte lineage. *Genesis* **50**, 506-515
447 (2012).
448 8. Etchevers, H.C., Vincent, C., Le Douarin, N.M. & Couly, G.F. The cephalic neural
449 crest provides pericytes and smooth muscle cells to all blood vessels of the face
450 and forebrain. *Development* **128**, 1059-1068 (2001).
451 9. Yu, Q.C., Song, W., Wang, D. & Zeng, Y.A. Identification of blood vascular
452 endothelial stem cells by the expression of protein C receptor. *Cell Res* **26**, 1079-
453 1098 (2016).
454 10. Wang, Y. *et al.* Ephrin-B2 controls VEGF-induced angiogenesis and
455 lymphangiogenesis. *Nature* **465**, 483-486 (2010).
456 11. Science, A.I.f.B. TECHNICAL WHITE PAPER: TRANSGENIC
457 CHARACTERIZATION. *Allen Brain Atlas* **9** (2015).
458 12. Kilani, B. *et al.* Comparison of endothelial promoter efficiency and specificity in
459 mice reveals a subset of Pdgfb-positive hematopoietic cells. *J Thromb Haemost*
460 **17**, 827-840 (2019).
461 13. Planas, A.M. Role of Immune Cells Migrating to the Ischemic Brain. *Stroke* **49**,
462 2261-2267 (2018).
463 14. Fernandez-Klett, F. *et al.* Early loss of pericytes and perivascular stromal cell-
464 induced scar formation after stroke. *J Cereb Blood Flow Metab* **33**, 428-439 (2013).
465 15. Piera-Velazquez, S. & Jimenez, S.A. Endothelial to Mesenchymal Transition: Role
466 in Physiology and in the Pathogenesis of Human Diseases. *Physiol Rev* **99**, 1281-
467 1324 (2019).

468 16. Hulshoff, M.S., Xu, X., Krenning, G. & Zeisberg, E.M. Epigenetic Regulation of
469 Endothelial-to-Mesenchymal Transition in Chronic Heart Disease. *Arterioscler*
470 *Thromb Vasc Biol* **38**, 1986-1996 (2018).

471